J Seismol (2019) 23:135–150
https://doi.org/10.1007/s10950-018-9797-y

ORIGINAL ARTICLE

Coulomb stress changes due to main earthquakes in Southeast Iran during 1981 to 2011

Behnam Maleki Asayesh · Hossein Hamzeloo · Hamid Zafarani

Received: 25 June 2016 / Accepted: 28 September 2018 / Published online: 25 October 2018

Abstract Southeast of Iran experienced eight destructive earthquakes during 30 years from 1981 to 2011. Six of these events with M > 6.5 were fatal and caused great human and financial losses in the region. The 1981 July 28 (Mw 7.2) Sirch earthquake with 65 km surface rupture was the largest event in this region since 1877 and with other three earthquakes occurred in Golbaf-Sirch region during 17 years. The 26 December 2003 (Mw 6.6) Bam earthquake was one of the most destructive events in the recorded history of Iran. There were more than 26,000 killed, 30,000 to 50,000 injured people, and more than 100,000 were homeless. We calculated the static coulomb stress changes due to this earthquake sequence (four earthquakes) between 1981 and 1998 on the Golbaf-Sirch right-lateral fault and the Shahdad reverse fault and a slow slip on the Shahdad fault. Our calculations showed positive stress changes due to previous events on the ruptured plane of next earthquake. For example, the rupture plane of the 14 March 1998 (Mw 6.6) Fandoqa earthquake received a maximum positive stress change about 2.3 MPa. Also, some parts of the surrounding faults received positive stress changes due to these events. Stress changes on the planes of other four events until 2011 were calculated in this study. The 26 December 2003 (Mw 6.6) Bam earthquake and the 20 December 2010 (Mw 6.5) first Rigan earthquake received negligible (about thousandth (0.001)) negative stress changes in this sequence. The last event in our study area, the 27 January 2011 (Mw 6.2) second Rigan earthquake, experienced more than 0.5 MPa coseismic coulomb stress changes especially in its hypocenter and according to our calculations, it is mostly due to the first Rigan event. By using well-located aftershocks of the Rigan earthquake, we investigated the correlation between coulomb stress changes and aftershocks distribution. Calculated coulomb stress changes due to these two events on the optimally oriented strike-slip faults for the first event showed that most of the well-located seismicity occurred in regions of stress increase and majority of them concentrated near the ruptured plane where the stress changes are in the highest value. Based on our computation for the second event, it would be concluded that most of the aftershocks located in the places that imposed stress are positive and some of them are in places where the imposed stress changes are zero or very small. So, there is a good correlation between coulomb stress changes and aftershocks distribution for both Rigan events. Calculating imparted coulomb stress changes that resolved on the nodal planes of the Rigan first event aftershocks has also been considered to examine whether they were brought closer to failure or not by using different fault friction. Various values of effective coefficient of friction (0.2, 0.4, and 0.8) were used to find the best value of fault friction that produces the highest gain in positively stressed aftershocks. Based on these calculations, majority of

B. Maleki Asayesh (✉) · H. Hamzeloo · H. Zafarani
International Institute of Earthquake Engineering and Seismology, (IIEES), Tehran, Iran
e-mail: b.m.asayesh@gmail.com

H. Zafarani
e-mail: h.zafarani@iiees.ac.ir

aftershocks received positive stress changes by increasing the effective coefficient of friction.

Keywords Earthquake · Coulomb stress change · Aftershock · Receiver fault · Southeast of Iran

1 Introduction

The active tectonic of Iran is dominated by the convergence of Arabian and Eurasian plates (Vernant et al. 2004). The crustal strain caused by the plate convergence is accommodated by inland active faults. Southeast of Iran with a large number of active faults such as the Kahorak, Jiroft, Golbaf, Kuh Banan, and Bam take part in accommodating of this strain.

It is reported by Ambraseys and Melville (2005) that 11 destructive historical earthquakes occurred in southeast of Iran, 7 of them with M > 6. The area has experienced about 50 earthquakes larger than 5 in the last 100 years (Maleki Asayesh and Hamzeloo 2015). The 2003 Mw 6.6 Bam earthquake that occurred in this area was responsible for the death of between 26,500 and 43,200 people and destruction of Bam City (Berberian 2005; Jackson et al. 2006; Talebian et al. 2004). Parts of the Golbaf-Sirch, Kuh Banan, Bam, and Rigan faults have been ruptured by eight earthquakes since 1981. Six of the mentioned earthquakes have magnitude equal to or more than 6.5 (Fig. 1 and Table 1).

The influence of static stress transfer due to moderate-to-large earthquakes on the location and occurrence time of future earthquakes is demonstrated by previous studies (e.g., Harris 1998; Stein 1999; King and Cocco 2001; Steacy et al. 2005a). Recent rate-state studies suggest that coseismic stress changes have a time-dependent effect on neighboring faults with an immediate jump in earthquake probability that decays with time (Parsons et al. 2000; Toda and Stein 2002; Toda et al. 2005).

The main objective of this study is to calculate the coulomb stress changes due to previous events on the fault plane of the next events. In fact, we intend to impart the coulomb stress changes caused by the previous events on the fault planes of the next events to see whether they were brought closer to failure or not. In addition, the correlation between coulomb stress changes of the Rigan dual earthquakes and spatial distribution of their aftershocks has been studied. Imparted stress

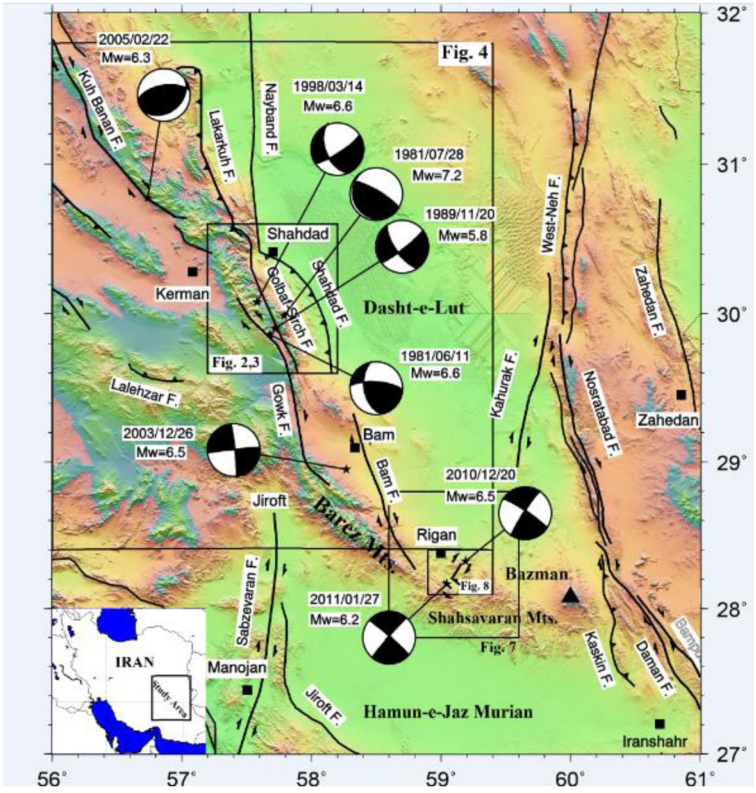

Fig. 1 Main tectonic features of southeast of Iran. Location and focal mechanism of the earthquakes that are used for stress calculation are shown (Berberian et al. 1984, 2001; Jackson et al. 2006; Rouhollahi et al. 2012; Walker et al. 2013; GCMT). Major cities are shown in black squares. The main active volcanic center, Bazman, is shown in black triangle. Faults are from Hessami et al. (2003). The solid black rectangles show the location of Figs. 2, 3, 4, 7, and 8

Table 1 Parameters of earthquake that are studied in this paper

Number	Earthquake	Date	Longitude	Latitude	Magnitude (M_w)	Depth (km)	Length (km)	Width (km)	Mean slip (m)	Moment ($*10^{18}$) N m	Nodal plane					
											Main plane			Axillary plane		
											Strike (°)	Dip (°)	Rake (°)	Strike (°)	Dip (°)	Rake (°)
1	Golbaf	1981 June 11	57.680[a]	29.860[a]	6.6[e]	20[e]	14[h,e]	15[h,e]	1.4[j]	09.48[e]	169[e]	52[e]	156[e]	274	71	040
			57.360	29.690	6.6	20	–	–	–	09.82	172	37	171	269	85	053
2	Sirch	1981 July 28	57.790[a]	29.990[a]	7.1[e]	18[e]	60[h,e]	16[h,e]	2.7[j]	36.69[e]	177[e]	69[e]	184[e]	086	86	159
			57.580	30.03	7.2	15.2	–	–	–	90.10	150	13	119	300	79	084
3	S. Golbaf	1989 November 20	57.720[a]	29.900[a]	5.8[e]	10[e]	10.2[h]	6.1[h]	0.22[j]	00.70[e]	145[e]	69[e]	188[e]	052	83	159
			57.800	29.890	5.8	15	–	–	–	0.81	148	81	165	240	75	009
4	Fandoqa	1998 March 14	57.580[a]	30.080[a]	6.6[e]	5[e]	23[h,e]	12.4[h,e]	1.7[j]	09.09[e]	156[e]	54[e]	195[e]	057	78	143
			57.600	29.950	6.6	15	–	–	–	09.43	154	57	174	061	85	033
5	Shahdad	1998 March 14	–	–	–	–	30[i]	20[i]	0.08[e]	02.00[e]	149[e]	06[e]	095[e]	324	84	086
			–	–	–	–	–	–	–	–	–	–	–	–	–	–
6	Bam	2003 December 26	58.268[b]	28.950[b]	6.6[f]	5.5[f]	20[h,f]	12[h,f]	2.14[f]	07.60[f]	354[f]	86[f]	182[f]	263	88	176
			58.240	29.100	6.6	15	–	–	–	09.31	172	59	167	269	79	031
7	Zarand	2005 February 22	56.736[c]	30.774[c]	6.5[g]	9[g]	18[g]	14[g]	1.4[j]	07.00[g]	260[g]	60[g]	104[g]	054	33	067
			56.810	30.760	6.0	25.4	–	–	–	05.20	266	47	100	071	44	079
8	Rigan1	2010 December 20	59.188[d]	28.325[d]	6.5[d]	5[d]	15[d]	13[d]	1.3[d]	07.10[d]	213[d]	85[d]	173[d]	304	83	005
			59.110	28.100	6.5	14.8	–	–	–	8.26	.36	87	180	126	90	003
9	Rigan2	2011 January 27	59.044[d]	28.169[d]	6.2[d]	9[d]	7[d]	17[d]	0.63[d]	02.60[d]	311	86	003	221	87	176
			59.020	28.020	6.2	14.3	–	–	–	2.42	129	77	− 005	221	85	− 167

Second row of each event shows the parameters of that event from CMT catalog (www.seismology.harvard.edu/)

[a] Engdahl et al. (1998)

[b] Engdahl et al. (2006)

[c] Talebian et al. (2004)

[d] Walker et al. (2013)

[e] Berberian et al. (2001)

[f] Jackson et al. (2006)

[g] Rouhollahi et al. (2012)

[h] Calculated based on the slip-seismic moment relation of Wells and Coppersmith (1994)

[i] Fielding et al. (2004)

[j] Based on empirical relation of Kanamori and Anderson (1975)

changes due to the 20 December 2010 event that resolved on its aftershocks nodal planes have also been calculated.

2 Seismotectonic setting

Active faulting, active folding, recent volcanic activities, mountainous terrain, and variable crustal thickness are characteristics of the Iranian Plateau. This plateau has been frequently struck by catastrophic earthquakes resulting in the massive loss of life, large masses homeless, and disrupting their agricultural and industrial lifelines (Berberian 1994, 1996). Based on Berberian (2005), the Iranian people have experienced at least one > 7.0 magnitude earthquake every 7 years, and one 6.0–6.9 magnitude earthquake every 2 years, during the twentieth century. And for the period of 1900 to 2005, more than 164,000 people have been killed by earthquakes in Iran.

As mentioned, Iran is subjected to a convergent stress produced by the motion of the Arabian plate in a NNE-SSW direction relative to the Eurasian plate. The crustal strain due to this plate convergence is accommodated by inland active faults and folds. GPS-derived velocities relative to the Eurasian plate infer that the plate motion in the central and eastern Iran is larger than in the west of Iran (the tectonic convergence rate in this area is about 8 mm year^{-1} in the direction of N8°E.) (Vernant et al. 2004). The lateral escape of central Iran with respect to the Lut Block is the result of indentation of the Arabian plate into a composite system of collision-oblique transpressive fold-thrust mountain belts (Berberian 2005).

The northward motion of central Iran relative to western Afghanistan results in two major fault zones that have been developed with a nearly north–south-oriented strike along the western and eastern borders of the Lut Block in eastern Iran (e.g., Freund 1970; Mohajer-Ashjai et al. 1975; Tirrul et al. 1983; Berberian and Yeats 1999; Walker and Jackson 2002). These faults with right-lateral motions reflect the subjected stress (Walker and Jackson 2004; Meyer and Le Dortz 2007).

Iranian plateau earthquakes are concentrated non-uniformly within the active fold-thrust mountain belts surrounding the relatively aseismic, undeformed rigid, and stable blocks. Based on Ambraseys and Melville (2005), Berberian (1981, 1994, 1995, 1996, 1997), and Berberian and Yeats (1999, 2001), the earliest earthquake in the Kerman-Bam plateau had been reported in 1854.

The Kuh Banan, Nayband, Gowk, Golbaf-Sirch, Bam, Sabzevaran, Kahurak, and Nosratabab strike-slip and Lakarkuh, Lalehzar, Shahdad, and West-Neh reverse faults are the main active faults of the study area in southeastern Iran, west and east of the Lut Desert (Fig. 1). The right-lateral shear along the western margin of the Lut block is directly transmitted between the Nayband, Lakarkuh, Kuh Banan, Gowk, Golbaf-Sirch, and Bam fault systems (Berberian 2005).

3 The coulomb stress triggering hypothesis

Earthquakes cause permanent deformation of the surrounding crust. They also change the stress on nearby faults as a function of their locations, geometry, and sense of slip (Toda et al. 2011). The coulomb failure function, ΔCFF, which is the coulomb stress change, depend on both changes in shear (Δτ) and normal stress (Δσ).

$$\Delta \mathrm{CFF} = \Delta\tau + \mu' \Delta\sigma \tag{1}$$

The parameter Δτ is the change in shear stress on the receiver fault (reckoned positive when sheared in the direction of fault slip), and Δσ is change in normal stress acting on the receiver fault (positive if the fault is unclamped) and μ′ is the apparent coefficient of friction which includes the unknown effect of pore pressure change as well (King et al. 1994; Mouyen et al. 2010). Depending on pore fluid content of the fault zone, μ′ changes between 0.2 and 0.8. Lower than 0.2 is suggested for well-developed and repeatedly ruptured fault zones because on these zones, sliding friction drops due to trapped pore fluids. On the other hand, higher than 0.8 amount can be used for young minor faults, since they did not have enough displacement for trapping pore fluids (King et al. 1994; Scholz 2002; Stein 1999; Steacy et al. 2004, 2005b).

Positive ΔCFF promotes failure and negative inhibits it; both increased shear and unclamping of faults are taken to promote failure, with the role of unclamping modulated by fault friction (Toda et al. 2011). Most of previous investigations of coulomb stress triggering (Harris 1998; Stein 1999; Freed 2005) found that static stress change plays an important role in the production

of aftershocks and subsequent mainshocks on surrounding faults (e.g., Harris 1998; Stein 1999; Freed 2005; Toda et al. 2011).

Studied events

As already mentioned, the southeast of Iran has experienced a number of destructive earthquakes during the last 35 years. Nine earthquakes occurred in the mentioned time frame are briefly elaborated in the following subsections. These events are considered to calculate the coulomb stress change in the southeast of Iran from 1981 till 2011 (Table 1).

3.1 Golbaf earthquake of 1981 June 11

The studied sequence is started by the 1981 June 11, Golbaf earthquake (Mw 6.6) which occurred on the southern part of the Golbaf-Sirch fault with a right-lateral surface rupture of approximately 15 km. This event killed more than 800 people and highly damaged all the villages in the Golbaf depression (Berberian et al. 1984). The epicenter of this event by NEIS is located at the northern part of the activated Golbaf fault segment (Berberian et al. 1984) but based on Engdahl et al. (1998), the epicenter was located at 29.86°N 57.68°E, in the west of the accompanied surface rupture (Fig. 2).

Surface displacements measured by Berberian et al. (1984) were quite small, typically with 3-cm right-lateral strike-slip and 5 cm vertical. Recalculated focal mechanism solution by Berberian et al. (2001) indicated right-lateral strike-slip faulting with a small normal faulting component (dipping west) striking NW–SE, parallel to the orientation of the Gowk fault in the area. They suggested a slip of about 75 cm for this event. We employ the slip-moment empirical relation of Kanamori and Anderson (1975), $u = \mathrm{Mo}/(\mathrm{LWG})$, where L and W are the fault length (km) and down-dip width (km), respectively, and G is the shear modulus (here 3.2×10^{10} N m^{-2}). For stress change calculation, we used slip of 140 cm by considering seismic moment of 9.48×10^{18} N m (Table 1).

3.2 Sirch earthquake of 1981 July 28

The second event that occurred approximately 1.5 months following the Golbaf event was the 1981 July 28 Sirch earthquake (Mw 7.2). This is a very challenging event that produced 65 km discontinuous surface rupture. This earthquake is considered as the largest event in the study area at least since 1877 (Berberian et al. 1984, 2001; Nalbant et al. 2006). Based on Engdahl et al. (1998), the epicenter of this event is located at 29.86°N 57.68°E, in the east of the southern end of its surface rupture (Fig. 2).

This event had a non-double-couple component of 30% and based on Berberian et al. (1984) began with a small sub-event preceding the main moment release by 4 s. This means the faulting was on at least two very different fault planes. First motion polarity studies all indicate a reverse faulting and GCMT solution indicate a 13-degree dipping thrust, dipping to the SW with strike of 150° that matches well with the Shahdad fault. Field studies showed only minor rupture of strike-slip and normal, and the intensity map did not show large intensities away from the observed rupture (Berberian et al. 1984). These observations indicate that the Sirch fault has not really ruptured during this event and just partially ruptured. In fact, the causative fault of this event is the Shahdad reverse fault and the observed motion along part of this fault during the 1998 Fandoqa earthquake can be considered as a remained part of the Sirch event.

Berberian et al. (1984) measured 65 km × 12 km fault plane and about 2.2 m average displacement for this earthquake. We used GCMT solution (Table 1) to calculate coulomb stress changes due to this earthquake. Based on Wells and Coppersmith (1994) empirical relations, subsurface rupture length of this earthquake is about 60 km and downdip rupture length is about 21 km. We also used 2.7 m mean slip from the slip-seismic moment relation of Kanamori and Anderson (1975).

3.3 South Golbaf earthquake of 1989 November 20

The 1989 November 20 (Mw 5.8) as the next event was a relatively small earthquake with 11 km of surface rupture. This earthquake followed the identical path of the scarps formed in the 11 June 1981 Golbaf earthquake (Berberian and Qorashi 1994; Berberian et al. 2001). As it is shown in the Fig. 2, the reported epicenter (29.90°N 57.72°E) for this event located at the northern end of the surface rupture of Golbaf 1981 June 11 earthquake (Engdahl et al. 1998). The inversion of P and SH waveforms by Berberian et al. (2001) confirmed that the event involved right-lateral strike-slip on a NNW–SSE nodal plane slightly dipping west. They also suggested ~0.4 m slip, and we calculated a mean slip

about 22 cm by using Kanamori and Anderson (1975) empirical relationship.

3.4 Fandoqa earthquake of 1998 march 14

The forth event in this sequence was the 1998 March 14 Fandoqa earthquake (Mw 6.6), which occurred on the Golbaf-Sirch fault and accompanied a 23-km-long surface rupture. This surface rupture includes re-rupturing of 19 km of the southernmost portion of the Sirch rupture and the gap left between the 1981 earthquakes. Due to this earthquake, nine people were killed and 15 were injured (Berberian et al. 2001). Based on Engdahl et al. (1998), the epicenter is at 30.08°N 57.58°E located in the northern end of its surface rupture (Fig. 2).

Field study of the surface rupture showed predominantly right-lateral strike-slip, distributed typically 1–2 m and reaches up to 3 m while the vertical offset was close to 1 m (Berberian et al. 2001). Analyzed P and SH body waveforms and SAR interferometry by Berberian et al. (2001) indicated a NW–SE rupture plane dipping to the west with an angle of 50°.

As an explanation for the overall rupture of Golbaf-Sirch fault system, the possibility of a ramp-and-flat thrust, but with strike-slip motion superimposed, was suggested by Berberian et al. (2001). So, the 1981 earthquake ruptured a deeper, flatter part of the system and the 1998 earthquake ruptured steeper and shallower fault later.

3.5 Shahdad event of 1998 March 14

Berberian et al. (2001) during the InSAR modeling of the Fandoqa earthquake recognized the March 14, 1998, Shahdad event, or triggered slip. Their InSAR modeling showed that there was an ~ 8 cm reverse motion on a very shallow SW dipping (6°) rectangular plane on the Shahdad thrust and folding system. Fielding et al. (2004) calculated slip on Shahdad plane by using a freely slipping boundary element that responded to the 1998 event, and they found approximately 7-cm reverse displacement over area of 30 km × 20 km extending from 1 to 4.5 km below the surface. Although this event in practice has very little influence on the stress change

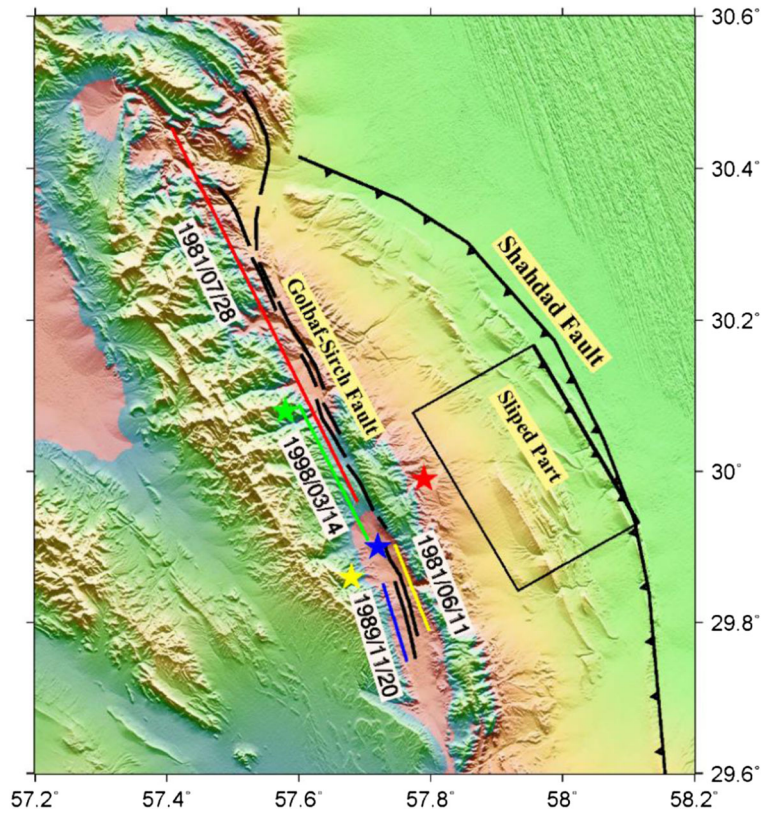

Fig. 2 Surface rupture on the Golbaf-Sirch fault system due to Golbaf, Sirch, South-Golbaf, and Fandoqa earthquakes. The rectangle shows the slipped part of the Shahdad fault on 1998 March 14 based on Berberian et al. (2001) and Fielding et al. (2004). The extent of surface rupture for each event is shown by a straight line which is colored based on the color of its epicenter

calculations, we include this slip in our modellings. The surface projection of the slipped part of the Shahdad fault is shown in Fig. 2.

3.6 Bam earthquake of 2003 December 26

The Bam earthquake (Mw 6.6) occurred on December 26, 2003. Based on Talebian et al. (2004), causative fault of this event is a blind fault that located approximately 4 km in the west of the previously mapped Bam fault.

The coseismic surface ruptures of this urban earthquake occurred on a near-vertical strike-slip fault within and south of the city of Bam. These ruptures involved at least five sub-parallel strike-slip fault segments and covered a width of approximately 4 km and a total length of 22.5 km (Berberian 2005; Jackson et al. 2006). Data from Envisat radar interferometry, InSAR, seismology, geomorphology, surface observations, and seismic body wave inversion showed a right-lateral, strike-slip mechanism on a nearly N–S striking vertical fault (Talebian et al. 2004; Wang et al. 2004; Jackson et al. 2006). Talebian et al. (2004) obtained a right-lateral strike-slip distribution on 2 km × 2 km grids, with a maximum of 2.5 m slip. Jackson et al. (2006) obtained an average slip of ~2.0 m mostly confined to depths between 2 and 8 km.

3.7 Dahuiyeh-Zarand earthquake of 2005 February 22

The 22 February 2005 (Mw 6.5) Dahuiyeh-Zarand earthquake occurred approximately 60 km away from the northern end of the surface rupture of the 1981 Sirch event and 280 km NW of the 2003 Bam earthquake. A reverse fault, striking nearly EW and dipping to the north, is located within a mountainous region recognized as a causative fault of this earthquake (Rouhollahi et al. 2012). Six three-component near-field strong motion waveforms were inverted by Rouhollahi et al. (2012) for obtaining the complete earthquake rupture history and slip distribution. Based on their study, the slip is found to be bilateral and the slip distribution on 2 km × 2 km grids showed a maximum slip of 2.4 m concentrated on two asperities in the west and east sides of the nucleation point at depths of 6–12 km (Fig. 5). Moreover, their final source model revealed a single reverse fault model with dimensions of 18 km × 14 km, strike 260°, dip 60° to the north with a nucleation point located at 9 km depth.

3.8 First Rigan earthquake of 2010 December 20

The last two events of our sequence occurred in the Rigan region in the southeast of studied area (south of Kerman province). The first Rigan event (Mw 6.5) occurred on 2010 December 20 in the southeast of Rigan city. Four children from a single family were killed in the small hamlet of Chah-Qanbar. This event caused several kilometers of surface rupture that was consistent with right-lateral slip on a fault striking ~40° (Walker et al. 2013). Walker et al. (2013) obtained a right-lateral focal mechanism with approximately vertical dip to the west by long-period body-waveforms modeling (Table 1). In addition, their InSAR analysis showed a right-lateral strike-slip distribution on 1 km × 1 km grids, with a maximum of 2.5 m slip and an average slip of ~1.3 m.

3.9 Second Rigan earthquake of 2011 January 27

Thirty-seven days after the first Rigan earthquake, another earthquake (Mw 6.2) struck the southwest of the first event on 2011 January 27. InSAR analysis and body-waveform modeling showed a NW-striking left-lateral mechanism (Table 1). Walker et al. (2013) found a slip model for this event with maximum of 1.1 m and average slip of 0.63 m.

Date, time, location, magnitude, parameters of nodal planes, and some of other information are summarized in Table 1 and shown in Fig. 1 (Engdahl et al. 1998; Engdahl et al. 2006; Talebian et al. 2004; Walker et al. 2013; Berberian et al. 2001; Jackson et al. 2006; Rouhollahi et al. 2012; Wells and Coppersmith 1994; Fielding et al. 2004; Kanamori and Anderson 1975). We have calculated some parameters that we could not find any references for them; for instance, we calculated length and width of some events (numbers 1, 2, 3, 4, and 6 in Table 1) based on the slip-seismic moment relation of Wells and Coppersmith (1994). In addition, the empirical relation of Kanamori and Anderson (1975) was applied to calculate mean slip of some events (numbers 1, 2, 3, and 4 in Table 1). The 'rake' computer code (Louvari and Kiratzi 1997) was also used to find the parameters of axillary plane.

4 Coulomb stress changes in the Southeast Iran sequence

This section starts with considering the first event as a source to calculate stress changes due to this event in the

ruptured plane of the next one. Then, the stress changes due to the last two events will be calculated in the ruptured plane of third event and this process is continued until the last one. Here, we used coulomb 3.4 software to calculate the coseismic static stress changes due to the earthquakes. Moreover, the Earth was assumed as a homogeneous elastic half-space and faults were considered as rectangular dislocations embedded within it. In order to consider these assumptions in our calculation, Young modulus, shear modulus, and Poisson ratio were considered equal to 8×10^5 bar, 3.2×10^5 bar, and 0.25, respectively.

It has proven difficult to discriminate among possible values of fault friction in coulomb stress transfer studies. High coefficient of friction (~ 0.8) was assumed for continental thrust faults and for young and normal faults, it may be superior. Moderate friction (0.4) was assumed for strike-slip or unknown faults. Low friction has been found to fit best for creeping faults, and very low friction (< 0.2) for major transforms, such as the San Andreas (Parsons et al. 1999; Toda and Stein 2002). So, a mid-value of 0.4 is most commonly adopted, and we considered this amount in our calculation for apparent coefficient of friction as it is close to friction for major faults (Harris and Simpson 1998; Parsons et al. 1999).

By considering the Golbaf earthquake of 1981 June 11 as a source, we calculated the static coulomb stress changes on the causative fault of Sirch earthquake of 1981 July 28. We used 1.4 m slip (Table 1) for the source fault and subdivided the assumed Sirch rectangular fault by 1 km × 1 km grids and obtained the transferred stress in each grid. Grids of this fault received coulomb stress changes with minimum of ~ − 0.369 MPa and maximum of ~ 0.028 MPa (Table 2 and Fig. 3a). The southern part of the Sirch rupture is located in the northern fault-end lob of coulomb stress changes and received the maximum amount of ΔCFF (more than 0.02 MPa) (Fig. 3a). This positive resolved stress has brought Sirch part of the fault closer to failure. Most of the surface rupture gap between these events that have not been ruptured during these earthquakes is placed where transferred stress due to Golbaf event decreases and stress changes have negative values (Fig. 3a).

In the second step, we calculated the static resolved stress due to Golbaf and Sirch earthquakes on the fractured plane in the South-Golbaf earthquake. For this part of calculation, we subdivided it into 60 1 km × 1 km grids and considered 1.4 m mean slip for the Golbaf event and 2.7 m for the Sirch event based on the empirical relation of Kanamori and Anderson (1975). The calculated stress showed a maximum increase about 3.51 MPa and maximum decrease about 3.86 MPa (Table 2). As it is shown in Fig. 3b, the south part of the South-Golbaf rupture received positive stress changes and the north part received negative stress changes. Based on King et al. (1994), positive stress changes about 0.1 bar (0.01 MPa) can bring faults to failure so this amount of transferred positive stress is sufficient to trigger the 20 November 1989 earthquake.

Afterward, we calculated static coulomb stress changes on the Fandoqa earthquake rupture resolved from the previous three events. For the Golbaf and Sirch events, we assumed same amount of slip that we had used for the South-Golbaf calculation and for the added South-Golbaf event, we used 22 cm displacement

Table 2 Minimum and maximum coulomb stress changes for ruptured faults in south east of Iran

Number	Earthquake	Fault name	Date	Coulomb stress changes (MPa)	
				Max.	Min.
1	Golbaf	Golbaf-Sirch	1981 June 11	–	–
2	Sirch	Golbaf-Sirch	1981 July 28	0.028	− 0.369
3	S. Golbaf	Golbaf-Sirch	1989 November 20	3.516	− 3.866
4	Fandoqa	Golbaf-Sirch	1998 March 14	2.309	− 0.506
5	Shahdad	Shahdad	1998 March 14	0.463	− 0.787
6	Bam	Bam	2003 December 26	− 0.019	− 0.188
7	Zarand	Kuh Banan	2005 February 22	0.003	0.002
8	Rigan1	Rigan1	2010 December 20	− 0.0004	− 0.002
9	Rigan2	Rigan2	2011 January 27	0.575	0.071

(Table 1). Like previous steps, we subdivided the Fandoqa rupture by 1 km × 1 km grids and our calculation showed about 2.3 MPa positive stress changes (Fig. 3c and Table 2). This high amount of positive transferred stress is sufficient for accumulating stress and causing the 14 March 1986 (Mw 6.6) earthquake in the region that had experienced two moderate and large events 17 years ago. Maximum amount of negative stress that transferred on this fault plane is about 0.5 MPa (Table 2).

Based on the previous studies such as Berberian et al. (2001) as well as the InSAR modeling of Fielding et al. (2004), it can be concluded that Shahdad fault has experienced approximately 8 cm reverse slip during the 1998 March 14 Fandoqa earthquake. Therefore, we calculated transferred stress on this fault due to the previous events and considered it as one of our sources for next calculations. By considering this plane as a receiver fault with the mechanism shown in Table 1, resolved stress on this reverse fault that was subdivided by 1 km × 1 km grids, which showed maximum positive amount about 0.46 MPa and maximum negative amount about − 0.78 MPa (Table 2). As it is shown in Fig. 3d, most parts of this plane received positive coulomb stress changes and one possible hypothesis is that this transferred stress triggered this part of Shahdad fault with reverse mechanism.

In all panels of Fig. 3, we observed lobes of increased stress at the source fault ends. These lobes of increased shear stress that concentrated at the fault ends tend to extend the fault, as it was discussed by King et al. (1994) and Das and Scholz (1981).

To investigate the transferred stress on the nearby faults, we calculated the coulomb stress changes due to these five events (Fig. 4). Lakarkuh fault with length of more than 130 km and north–south direction is a reverse fault with a right-lateral component (Hessami et al. 2003). The southern end of this fault is located in the boundary of positive and negative stress changes lobes (Fig. 4a). Based on Nabavi (1976) and Aghanabati

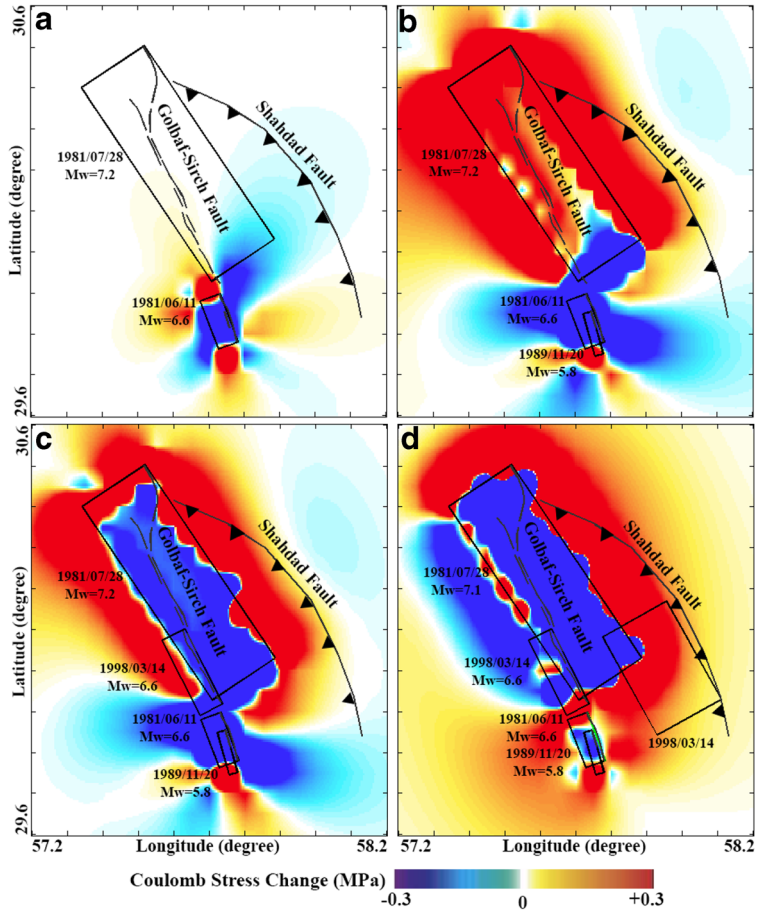

Fig. 3 Calculated coulomb stress changes due to earthquakes occurred on the Golbaf, Sirch, and Shadad regions. **a** Coulomb stress change due to Golbaf 1981 June 11 event on the Sirch event ruptured plane, which is considered as receiver fault. **b** Transferred stress on the South-Golbaf ruptured plane due to Golbaf and Sirch events. **c** The ruptured plane of the Fandoqa event is considered as a receiver and the three previous events are considered as sources. **d** In this picture, transferred stress due to the previous events on the slipped part of Shahdad fault on the 14 March 1998 is shown. The depth of all calculation is 10 km

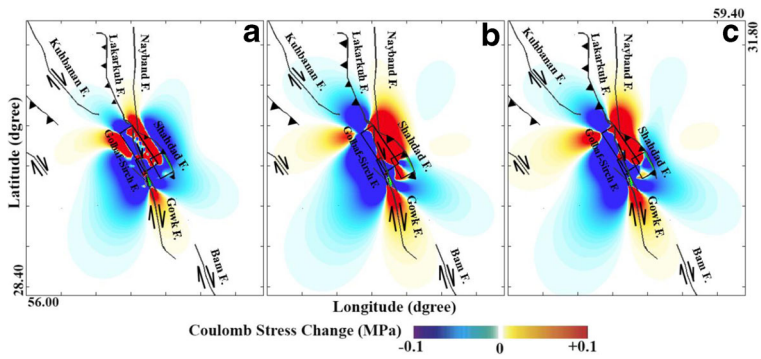

Fig. 4 Coulomb stress changes due to Golbaf, Sirch, South-Golbaf, Fandoqa, and Shahdad slips on the surrounding faults. **a** The receiver fault is Lakarkuh fault at depth of 7.5 km. **b** The receiver fault is Nayband fault at depth of 7.5 km. **c** The receiver fault is Gowk fault at depth of 7.5 km

(2004), the Nayband fault with north–south strike and about 600 km length is a right-lateral strike-slip fault. This fault with dip of about 80° received large amount of positive coulomb stress changes in the southern end (Fig. 4b). In the south of these five events. we have Gowk fault with NNW–SSE strike. Majority of its 150-km length is right-lateral strike-slip fault (Berberian and Qorashi 1994; Walker and Jackson 2004) and located in the place that received positive stress changes (Fig. 4c). So, some parts of the surrounding faults received positive stress changes due to Golbaf, Sirch, South-Golbaf, Fandoqa, and Shahdad slips.

After 5 years, the city of Bam which is 100 km far from the southeast of Golbaf-Sirch fault system experienced one of the most destructive earthquakes in history of Iran. The calculated coulomb stress changes on the fault plane of this event due to the five previous earthquakes showed a little negative amount (Table 2). This little effect can be attributed to the abovementioned large distance. In the next step, the Bam earthquake is added as a source, in order to calculate the coulomb stress changes on the Zarand ruptured plane as a reverse fault. We considered right-lateral variable-slip for the Bam rupture (Fig. 5a) based on the Talebian et al. (2004) model. Transferred stress on all grids of Zarand fault has positive amount with maximum 0.003 MPa (Table 2). It is obvious that slip on the Bam fault has a little effect on the Zarand rupture because of more than 200 km distance. We have also calculated the coulomb stress changes without considering Bam earthquake slip and observed it decreases about thousandth (0.001) bar.

In the following step, we added the Dahuiyeh-Zarand earthquake as a source in our calculation. The variable-slip on this reverse event was calculated and added to input files based on Rouhollahi et al. (2012) (Fig. 5b), and the resolved stress due to this earthquake and previous events on the first Rigan earthquake was calculated (Table 2). The calculated coulomb stress changes were negative and minor. As the Bam earthquake was

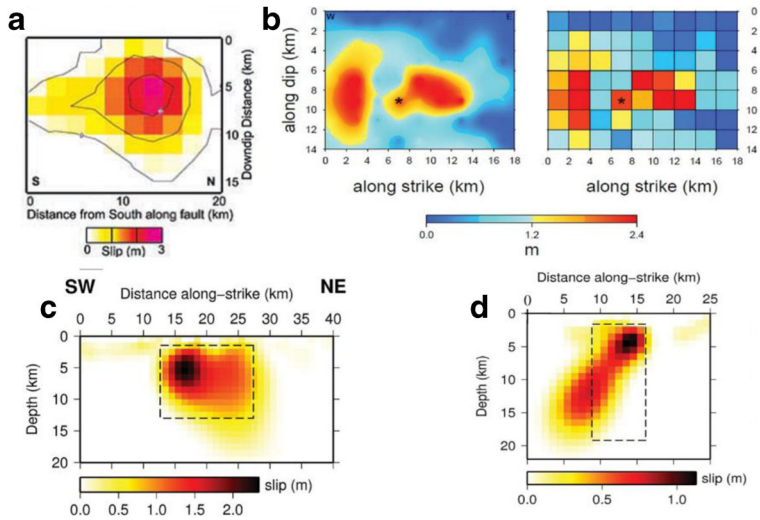

Fig. 5 Variable-slip for calculating coulomb stress changes. **a** Distribution of slip on the main right-lateral strike-slip Bam fault (Talebian et al. 2004). **b** Slip distribution on the causative fault of Dahuiyeh-Zarand earthquake (Rouhollahi et al. 2012). **c** Slip distribution on the first Rigan earthquake fault plane from variable-slip fault model (Walker et al. 2013). **d** Slip distribution on the second Rigan earthquake fault plane from variable-slip fault model (Walker et al. 2013)

the nearest event to the Rigan rupture, we resolved the stress only due to Bam earthquake on this fault. Obtained results showed a little increase in the resolved stress that could not be changed to positive amount.

Then, we calculated the transferred stress on the second Rigan event. For this purpose, we added the right-lateral variable-slip of the first Rigan event to our calculations based on the slip model presented in Walker et al. (2013) (Fig. 5c). The transferred stress on the second Rigan rupture showed maximum stress changes about 0.57 MPa (Table 2). By calculating the transferred stress due to the first Rigan event on the second Rigan rupture plane (Fig. 7a), we found out that majority of this transferred stress is because of the first Rigan event and previous events increased it only ~ 0.003 MPa. This resolved stress on the second Rigan plane advanced the 6.2 magnitude earthquake on the fault with left-lateral mechanism.

We also calculated that transferred stress due to all events (9 slips) on the surrounding faults by considering general trend of the faults in the study area (NNW–SSE) as a receiver fault (Fig. 6). The results showed positive stress changes in the southern ends of the Nayband, Lakarkuh, and Bam faults, and also in the northern and the southern ends of the Gowk fault. Also, southern part of the Kuh Banan fault received positive stress changes. These regions that received positive stress changes are the hazardous and probable places for the future events.

5 Correlating coulomb stress changes and aftershocks

Availability of a well relocated aftershocks (RMS < 2.5 s) for the first Rigan and the second Rigan earthquakes (Walker et al. 2013; Maleki et al. 2012; Reza et al. 2013), enable us to calculate coulomb stress changes due to these two earthquakes on optimally orientated fault planes for investigating correlation between coulomb stress changes and aftershock distribution.

After the first Rigan event (Mw 6.5), more than 1300 aftershocks were recorded by the broadband and the temporary networks of the International Institute of Earthquake Engineering and Seismology (IIEES), and the temporary and permanent networks of the Iranian Seismological Center (IRSC) at the Institute of Geophysics of Tehran University during 1 month (Reza

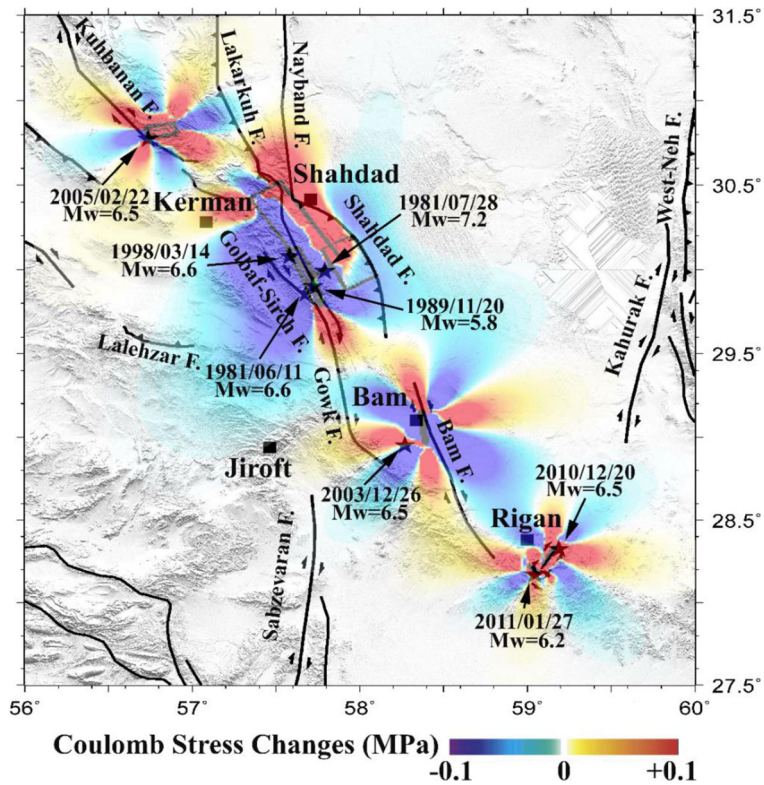

Fig. 6 Coulomb stress change due to nine slips on the general trend of the faults at the depth of 7.5 km

et al. 2013). In this part of study, we used a combination set of aftershocks from three different sets. Maleki et al. (2012) relocated about 80 aftershocks for the first event of Rigan using non-linear method. They only relocated aftershocks that had been recorded at least in five stations. Walker et al. (2013) relocated more than 20 aftershocks of this earthquake by using a relocation method based on the hypocentroidal decomposition (HDC) method for multiple events relocation (Jordan and Sverdrup 1981). The third set of relocated aftershocks was taken from Reza et al. (2013). They relocated about 550 aftershocks that had been recorded at least in five stations by using a local crustal model. By combining these catalogs, we prepared more than 600 well-located aftershocks for the first Rigan event. Also, we prepared about 130 well-relocated aftershocks based on Walker et al. (2013) and Maleki et al. (2012) for the second event.

In addition to parameters describing fault geometry (e.g., location and dip angle), elastic properties of the material (E, Young's modulus; m, Poisson's ratio; μ′, coefficient of friction), and the amount of slip on the

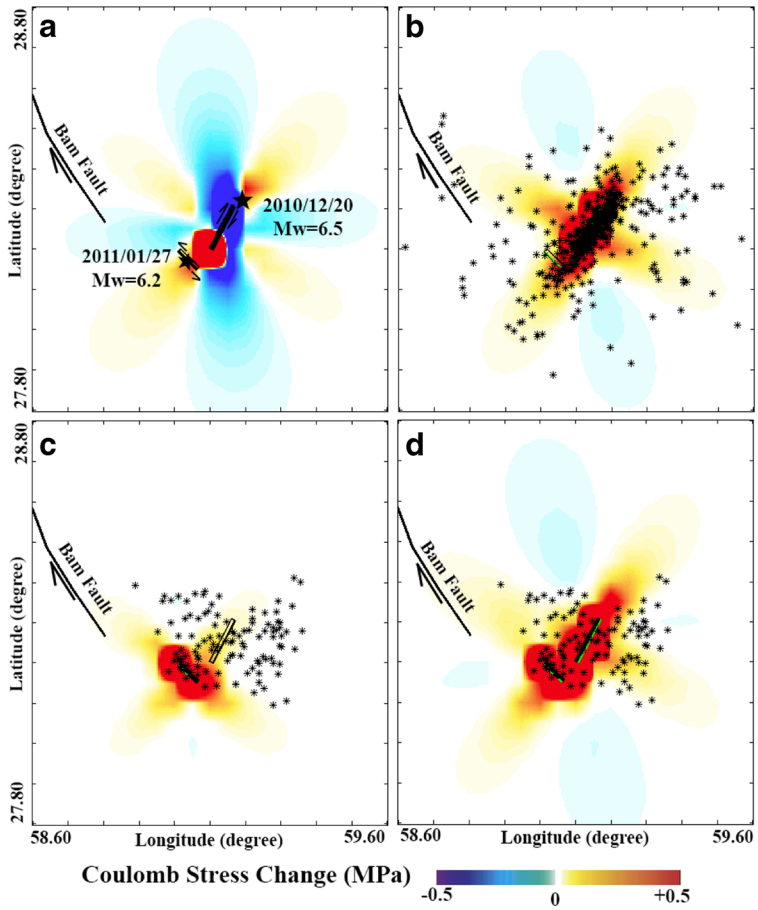

Fig. 7 Coulomb stress changes and seismicity. **a** Coulomb stress changes due to the 20 December 2010 earthquake on the 27 January 2011 earthquake plane. The calculation had been computed at depth of 9 km, and the fault of the 27 January 2011 event is assumed as a receiver plane. Black stars show the epicenter of the Rigan main shocks, black lines show surface projection of ruptured planes, and arrows show kind of slip on the planes. **b** Maximum resolved stress changes on the optimally oriented strike-slip faults due to the 20 December 2010 (Mw 6.5) earthquake for depth range of 0.0–20.0 km and distribution of well-located aftershocks (Walker et al. 2013; Reza et al. 2013; Maleki et al. 2012) that occurred until the 27 January 2011 earthquake during 37 days. **c** Map view of maximum stress change for depth range of 0.0–20 km due to the 27 January 2011 earthquake on the optimally oriented strike-slip faults with seismicity (during 6 months) from Walker et al. (2013) and Maleki et al. (2012). **d** Map view of maximum stress change for depth range of 0.0–20 km due to the 20 December 2010 and the 27 January 2011 earthquakes on the optimally oriented strike-slip faults with seismicity (during 6 months) from Walker et al. (2013) and Maleki et al. (2012)

fault, an estimate of the regional stress field is necessary to model the coulomb stress changes on optimal orientations. We used variable-slip based on Walker et al. (2013) in our calculation (Fig. 5). A maximum stress oriented in N 8° E ± 5° by Vernant et al. (2004) is used for this region. They estimated about 8 mm tectonically convergent rate in the mentioned direction based on GPS measurements.

We calculated coulomb stress changes due to the first Rigan event on the optimally oriented strike-slip faults (Fig. 7b), and it revealed that most of the well-located seismicity occurred in regions of stress increase. Majority of seismicity concentrated near the ruptured plane where the stress changes are high. The rest of the aftershocks are also placed in the region with positive stress changes, so there is a good correlation between coulomb stress changes due to the 20 December 2010 event and location of its aftershocks until 27 January 2011 during 37 days.

To investigate a probable correlation between this event and seismicity, we used 135 well-located aftershocks during 7 months after this event based on Walker et al. (2013) and Maleki et al. (2012). For this purpose, we used left-lateral variable-slip model (Fig. 5) for 27 January 2010 earthquake. Our computation showed that some of these aftershocks located in the places that experienced stress increases and some of them are in places where the imposed stress changes are zero or very small (Fig. 7c). The effect of the first Rigan earthquake on the distribution of the aftershocks occurred after 27 January 2011 is not negligible due to the relatively short temporal and spatial distances. By calculating the coulomb stress changes due to both Rigan earthquakes, it is observed that the majority of aftershocks are located where the stress changes are positive and very few of them are located in places with no stress changes (Fig. 7d). As a result, we conclude that there is a good correlation between coulomb stress changes due to both Rigan events and seismicity after these events.

6 Coulomb stress changes on the nodal planes of 20 December 2010 Rigan earthquake

We calculated imparted coulomb stress changes that resolved on the nodal planes of the first Rigan event aftershocks by using different fault friction to examine whether they were brought closer to failure or not and in which amount of friction coefficient the resolved stress changes on nodal planes are more.

We used 28 aftershocks with available focal mechanisms in Walker et al. (2013) and Reza et al. (2013). These events occurred from 24 December 2010 to 28 January 2011; magnitude ranges from 2.9 to 6.2 within the depth range of 0–20 km.

We used the source model of the 20 December 2010 main-shock that was derived by Walker et al. (2013) (P, SH, body, and InSAR analysis), as noted in Table 1 and Fig. 5. We used multiple effective friction coefficients (0.2, 0.4, and 0.8) to find the best value of fault friction that produces the highest gain in positively stressed aftershocks. By using 0.2 as an effective friction coefficient, it is revealed that about 32% (9 of 28) of aftershock nodal planes received positive stress changes. For $\mu' = 0.4$ it was 46.42% (13 of 28) and for $\mu = 0.8$, it is shown about 67.85% (19 of 28) aftershocks received positive stress changes (Fig. 8).

7 Conclusion

The stress interaction relationship among the $M \geq 6.0$ events occurred in the southeast of Iran since 1981 has been investigated. We considered nine events as sources and calculated coulomb stress changes due to these events. The Golbaf-Sirch region showed clear stress load to failure relationship. Since we did not consider any earthquakes before the 11 June 1981 Golbaf event, we could not calculate coulomb stress changes imparted on the rupture plane of this event. Up to 0.02 MPa coulomb stress was imparted due to failure of this event upon the fault plane of the 1981 Sirch earthquake, which most likely advanced the event. The gap between the surface ruptures of these two events received positive stress change, and this may explain why it finally ruptured. Static coulomb stress due to the Golbaf and Sirch earthquakes on the South-Golbaf plane showed large amount of increase (3.5 MPa) and large amount of decrease (3.8 MPa). This high increased stress advanced the 20 November of 1989 earthquake.

The 1998 Fandoqa earthquake accompanied a 23-km-long surface rupture; 19 km of that overlapped with the southern part of the Sirch rupture plane and 6.6 km of that corresponded with the gap among the 1981 earthquakes. Calculated static coulomb stress changes on the Fandoqa earthquake ruptured plane due to previous events showed about 2.3 MPa positive stress

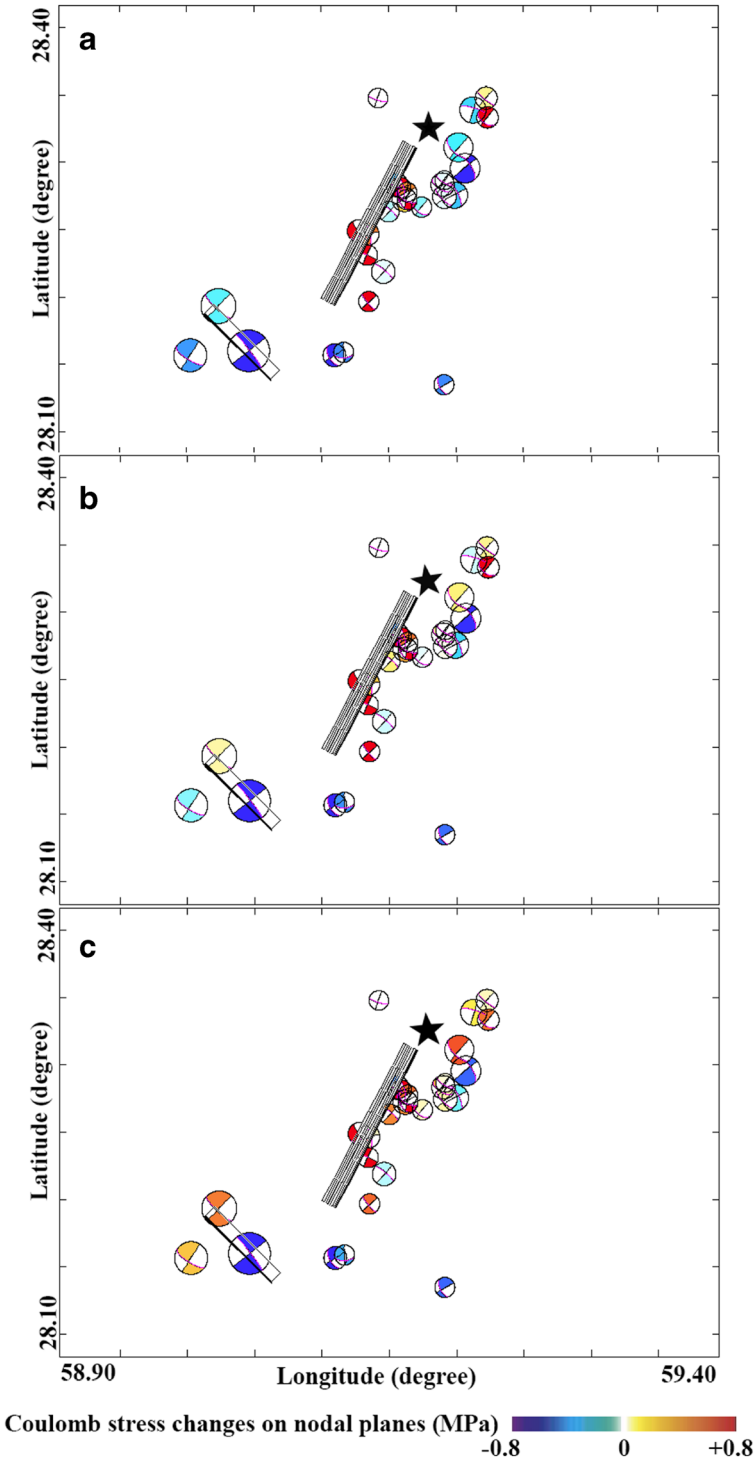

Fig. 8 Stress imparted by the 20 December 2010 Rigan earthquake on the nodal planes of its aftershocks. The coefficient values are in turn **a** $\mu' = 0.2$, **b** $\mu = 0.4$, and **c** $\mu' = 0.8$. The black star shows the epicenter of the mainshock

changes, and it brought this part of the Golbaf-Sirch fault to failure. The 16-km-long part of this rupture that ruptured in the Sirch event showed negative amount with maximum of more than 0.5 MPa. Coseismic stress changes due to earthquakes occurred on the Golbaf-Sirch region on the 1998 Shahdad ruptured plane which showed maximum positive amount about 4.6 MPa. Some parts of the surrounding faults received positive

stress changes due to Golbaf, Sirch, South-Golbaf, Fandoqa, and Shahdad events.

Transferred stress on Bam fault plane due to five previous earthquakes showed a small negative amount. This little effect is due to large distance. Calculated coulomb stress changes on the Zarand ruptured plane as a reverse event was about 0.02 MPa. The imparted stress due to the first seven slips in the southeast of Iran on the Rigan dual earthquakes was negligible and negative. This was due to large distance. However, the first Rigan earthquake imparted about + 0.57 MPa stress on the rupture plane of the second Rigan earthquake.

Aftershock location of the first Rigan earthquake correlated well with areas of increased coulomb stress changes following the mainshock. Majority of well-located seismicity concentrated near the ruptured plane where the stress changes are high. Also, majority of the aftershocks following the second Rigan earthquake distributed where the coulomb stress changes due to this event were positive; moreover, they showed good relationships with the stress changes due to both Rigan earthquakes. Furthermore, a friction coefficient of 0.8 better manifests the imparted coulomb stress on the favorable nodal planes of the aftershocks.

Transferred stress due to all events on the surrounding faults has been calculated, and the results revealed that southern ends of the Nayband, Lakarkuh, and Bam faults; northern and southern ends of the Gowk fault; and also southern part of the Kuh Banan fault received positive stress changes. These regions should be considered as the hazardous and probable places for the future events.

Acknowledgements We thank Mona Reza, Gholam Javan, and Vahid Maleki for allowing us to use their relocated aftershocks. We also are grateful to anonymous reviewers for their reviews and comments, which significantly improved this article.

References

Aghanabati A (2004) Geology of Iran. Geological survey of Iran

Ambraseys NN, Melville CP (2005) A history of Persian earthquakes. Cambridge university press, Cambridge

Berberian M (1981) Active faulting and tectonics of Iran. Zagros-Hindu Kush-Himalaya Geodynamic Evolution 3:33–69

Berberian M (1994) Natural hazards and the first earthquake catalogue of Iran. International Institute of Earthquake Engineers and Seismology

Berberian M (1995) Master "blind" thrust faults hidden under the Zagros folds: active basement tectonics and surface morphotectonics. Tectonophysics 241(3–4):193–224

Berberian M (1996) The historical record of earthquakes in Persia, Encyclopaedia Iranica, VII F. 6, Drugs-Ebn al-Atir

Berberian M (1997) Seismic sources of the Transcaucasian historical earthquakes. Historical and prehistorical earthquakes in the Caucasus, 28, pp 233–311

Berberian M (2005) The 2003 bam urban earthquake: a predictable seismotectonic pattern along the western margin of the rigid Lut block, Southeast Iran. Earthquake Spectra 21(S1): 35–99

Berberian M, Qorashi M (1994) Coseismic fault-related folding during the south Golbaf earthquake of November 20, 1989, in Southeast Iran. Geology 22(6):531–534

Berberian M, Yeats RS (1999) Patterns of historical earthquake rupture in the Iranian plateau. Bull Seismol Soc Am 89(1): 120–139

Berberian M, Yeats RS (2001) Contribution of archaeological data to studies of earthquake history in the Iranian plateau. J Struct Geol 23(2–3):563–584

Berberian M, Jackson JA, Ghorashi M, Kadjar MH (1984) Field and teleseismic observations of the 1981 Golbaf–Sirch earthquakes in SE Iran. Geophys J Int 77(3):809–838

Berberian M, Jackson JA, Fielding E, Parsons BE, Priestly K, Qorashi M, Talebian M, Walker R, Wright TJ, Baker E (2001) The 1998 March 14 Fandoqa earthquake (Mw6.6) in Kerman, Southeast Iran: re-rupture of the 1981 Sirch earthquake fault, triggering of slip on adjacent thrusts, and the active tectonics of the Gowk fault zone. Geophys J Int 146(2):371–398

Das S, Scholz CH (1981) Off-fault aftershock clusters caused by shear stress increase? Bull Seismol Soc Am 71(5):1669–1675

Engdahl ER, van der Hilst R, Buland R (1998) Global teleseismic earthquake relocation with improved travel times and procedures for depth determination. Bull Seismol Soc Am 88(3): 722–743

Engdahl ER, Jackson JA, Myers SC, Bergman EA, Priestley K (2006) Relocation and assessment of seismicity in the Iran region. Geophys J Int 167(2):761–778

Fielding EJ, Wright TJ, Muller J, Parsons BE, Walker R (2004) Aseismic deformation of a fold-and-thrust belt imaged by synthetic aperture radar interferometry near Shahdad, Southeast Iran. Geology 32(7):577–580

Freed AM (2005) Earthquake triggering by static, dynamic, and postseismic stress transfer. Annu Rev Earth Planet Sci 33: 335–367

Freund R (1970) Rotation of strike slip faults in Sistan, Southeast Iran. The Journal of Geology 78(2):188–200

Harris RA (1998) Introduction to special section: stress triggers, stress shadows, and implications for seismic hazard. J Geophys Res Solid Earth 103(B10):24347–24358

Harris RA, Simpson RW (1998) Suppression of large earthquakes by stress shadows: a comparison of Coulomb and rate-and-state failure. J Geophys Res Solid Earth 103(B10):24439–24451

Harvard Seismology (2017) Centroid moment tensor (CMT) catalog search, www.seismology.harvard.edu/. Accessed Dec 2017

Hessami K, Jamali F and Tabasi H (2003) Major active faults map of Iran, scale 1: 2500000. International Institute of Earthquake Engineering and Seismology

Jackson J, Bouchon M, Fielding E, Funning G, Ghorashi M, Hatzfeld D, Nazari H, Parsons B, Priestley K, Talebian M, Tatar M (2006) Seismotectonic, rupture process, and earthquake-hazard aspects of the 2003 December 26 Bam, Iran, earthquake. Geophys J Int 166(3):1270–1292

Jordan TH, Sverdrup KA (1981) Teleseismic location techniques and their application to earthquake clusters in the south-Central Pacific. Bull Seismol Soc Am 71(4):1105–1130

Kanamori H, Anderson DL (1975) Theoretical basis of some empirical relations in seismology. Bull Seismol Soc Am 65(5):1073–1095

King GCP, Cocco M (2001) Fault interaction by elastic stress changes: new clues from earthquake sequences. Adv Geophys 44:1–VIII

King GC, Stein RS, Lin J (1994) Static stress changes and the triggering of earthquakes. Bull Seismol Soc Am 84(3):935–953

Louvari EK, Kiratzi AA (1997) Rake: a Windows program to plot earthquake focal mechanisms and the orientation of principal stresses. Comput Geosci 23(8):851–857

Maleki Asayesh B and Hamzeloo H (2015) Coulomb stress changes due to Rigan earthquakes and distribution of aftershocks. Bulletin of Earthquake Science and Engineering 2(2)

Maleki V, Shomali ZH, Hatami MR (2012) Relocation of the aftershocks of Mohamad Abad Rigan earthquake December 20, 2010, (Mn = 6.5) using a nonlinear method. Iranian Journal of Geophysics 6(4):96–111

Meyer B and Le Dortz K (2007) Strike-slip kinematics in central and eastern Iran: estimating fault slip-rates averaged over the Holocene. Tectonics 26(5)

Mohajer-Ashjai A, Behzadi H, Berberian M (1975) Reflections on the rigidity of the Lut block and recent crustal deformation in eastern Iran. Tectonophysics 25(3–4):281–301

Mouyen M, Cattin R, Masson F (2010) Seismic cycle stress change in western Taiwan over the last 270 years. Geophys Res Lett 37(3)

Nabavi MH (1976) Preface geology of Iran. Geology Survey, Iran

Nalbant SS, Steacy S, McCloskey J (2006) Stress transfer relations among the earthquakes that occurred in Kerman province, southern Iran since 1981. Geophys J Int 167(1):309–318

Parsons T, Stein RS, Simpson RW, Reasenberg PA (1999) Stress sensitivity of fault seismicity: a comparison between limited-offset oblique and major strike-slip faults. J Geophys Res Solid Earth 104(B9):20183–20202

Parsons T, Toda S, Stein RS, Barka A, Dieterich JH (2000) Heightened odds of large earthquakes near Istanbul: an interaction-based probability calculation. Science 288(5466):661–665

Reza M, Abbasi MR, Javan-Doloei G, Sadidkhuy A (2013) Identifying fault of Mohammad Abad Rigan 20/12/2010 earthquake and its focal mechanism using aftershock analyses. Iranian Journal of Geophysics 8(1):59–70

Rouhollahi R, Ghayamghamian MR, Yaminifard F, Suhadolc P, Tatar M (2012) Source process and slip model of 2005 Dahuiyeh-Zarand earthquake (Iran) using inversion of near-field strong motion data. Geophys J Int 189(1):669–680

Scholz CH (2002) The mechanics of earthquakes and faulting. Cambridge university press, Cambridge

Steacy S, Marsan D, Nalbant SS, McCloskey J (2004) Sensitivity of static stress calculations to the earthquake slip distribution. J Geophys Res Solid Earth 109(B4)

Steacy S, Gomberg J, Cocco M (2005a) Introduction to special section: stress transfer, earthquake triggering, and time-dependent seismic hazard. J Geophys Res Solid Earth 110(B5)

Steacy S, Nalbant SS, McCloskey J, Nostro C, Scotti O, Baumont D (2005b) Onto what planes should coulomb stress perturbations be resolved? J Geophys Res Solid Earth 110(B5)

Stein RS (1999) The role of stress transfer in earthquake occurrence. Nature 402(6762):605

Talebian M, Fielding EJ, Funning GJ, Ghorashi M, Jackson J, Nazari H, Parsons B, Priestley K, Rosen PA, Walker R, Wright TJ (2004) The 2003 Bam (Iran) earthquake: rupture of a blind strike-slip fault. Geophys Res Lett 31(11)

Tirrul R, Bell IR, Griffis RJ, Camp VE (1983) The Sistan suture zone of eastern Iran. Geol Soc Am Bull 94(1):134–150

Toda S, Stein RS (2002) Response of the San Andreas fault to the 1983 Coalinga-Nunez earthquakes: an application of interaction-based probabilities for Parkfield. J Geophys Res Solid Earth 107(B6)

Toda S, Stein RS, Richards-Dinger K, Bozkurt SB (2005) Forecasting the evolution of seismicity in southern California: animations built on earthquake stress transfer. J Geophys Res Solid Earth 110(B5)

Toda S, Lin J, Stein RS (2011) Using the 2011 Mw 9.0 off the Pacific coast of Tohoku earthquake to test the coulomb stress triggering hypothesis and to calculate faults brought closer to failure. Earth, Planets and Space 63(7):39

Vernant P, Nilforoushan F, Hatzfeld D, Abbassi MR, Vigny C, Masson F, Nankali H, Martinod J, Ashtiani A, Bayer R, Tavakoli F (2004) Present-day crustal deformation and plate kinematics in the Middle East constrained by GPS measurements in Iran and northern Oman. Geophys J Int 157(1):381–398

Walker R, Jackson J (2002) Offset and evolution of the Gowk fault, SE Iran: a major intra-continental strike-slip system. J Struct Geol 24(11):1677–1698

Walker R, Jackson J (2004) Active tectonics and late Cenozoic strain distribution in central and eastern Iran. Tectonics 23(5)

Walker RT, Bergman EA, Elliott JR, Fielding EJ, Ghods AR, Ghoraishi M, Jackson J, Nazari H, Nemati M, Oveisi B, Talebian M (2013) The 2010–2011 south Rigan (Baluchestan) earthquake sequence and its implications for distributed deformation and earthquake hazard in Southeast Iran. Geophys J Int 193(1):349–374

Wang R, Xia Y, Grosser H, Wetzel HU, Kaufmann H, Zschau J (2004) The 2003 Bam (SE Iran) earthquake: precise source parameters from satellite radar interferometry. Geophys J Int 159(3):917–922

Wells DL, Coppersmith KJ (1994) New empirical relationships among magnitude, rupture length, rupture width, rupture area, and surface displacement. Bull Seismol Soc Am 84(4):974–1002